

Effects of charge-density-wave phase transition on electrical transport and Raman spectra in 2H-tantalum disulfide

Cite as: Appl. Phys. Lett. **114**, 141901 (2019); <https://doi.org/10.1063/1.5086951>

Submitted: 26 December 2018 . Accepted: 13 March 2019 . Published Online: 12 April 2019

Kai Zhang , Zi-Yu Cao, and Xiao-Jia Chen



View Online



Export Citation



CrossMark

Applied Physics Reviews
Now accepting original research

2017 Journal
Impact Factor:
12.894

AIP
Publishing

Effects of charge-density-wave phase transition on electrical transport and Raman spectra in $2H$ -tantalum disulfide

HPSTAR
742-2019

Cite as: Appl. Phys. Lett. **114**, 141901 (2019); doi: [10.1063/1.5086951](https://doi.org/10.1063/1.5086951)
Submitted: 26 December 2018 · Accepted: 13 March 2019 ·
Published Online: 12 April 2019



View Online



Export Citation



CrossMark

Kai Zhang,^{1,2,3}  Zi-Yu Cao,^{1,2,3} and Xiao-Jia Chen^{3,a)}

AFFILIATIONS

¹Key Laboratory of Materials Physics, Institute of Solid State Physics, Chinese Academy of Sciences, Hefei 230031, China

²University of Science and Technology of China, Hefei 230026, China

³Center for High Pressure Science and Technology Advanced Research, Shanghai 201203, China

^{a)}Electronic mail: xjchen@hpstar.ac.cn

ABSTRACT

Measurements of electrical transport and Raman spectroscopy are performed on $2H$ -TaS₂ to study the formation and the character of the charge density wave. The entry of the charge-density-wave state below the lock-in temperature is detected by the sudden change of the resistivity slope with temperature, the sharp rise of the magneto-resistivity, and the significant change in the Hall coefficient. Meanwhile, the frequency of the two-phonon mode decreases with decreasing temperature. When approaching the lock-in temperature, the formation of the charge density wave is also evidenced by the disappearance of the two-phonon mode. In the charge density wave state, the newly born charge-density-wave modes in the E_{2g} - and A_{1g} -symmetries exhibit a blue-shift with decreasing temperature. These results suggest that the combined techniques of electrical transport measurement and Raman spectroscopy are powerful in studying the charge-density-wave order in materials with strong electron-phonon coupling.

Published under license by AIP Publishing. <https://doi.org/10.1063/1.5086951>

Transition metal dichalcogenides (TMDs), with the van der Waals force connected layered structure, have great significance in application and scientific research in many fields.¹ They, especially the $2H$ -polytype TMDs, always show complex electronic behaviors such as charge density wave (CDW) orders.² This makes them potential candidate materials for studying the origin of the lattice instability, as well as the interaction between CDW and superconductivity for which a competitive relationship has been demonstrated to exist.^{3–5} The CDW orders were found to be general in many cuprate superconductors.^{6–8} These high temperature superconductors almost share the similar phase diagram with TMDs.^{9,10} The study of the relationship between superconductivity and CDW is useful for understanding the unsolved mechanism of superconductivity. However, to date, the reason for CDW formation is still shrouded in mystery. It has been proposed by several hypotheses, such as saddle-point,^{11,12} Fermi-surface (FS) nesting,^{10,13,14} q -dependent electron-phonon coupling,^{15–20} etc. The former two have been excluded because of the inappropriateness in explaining their origin.^{15,16,21–23} The electron-phonon interaction mechanism becomes the most persuasive standpoint. This mechanism has certified by a lot of angle-resolved photoemission spectroscopy

measurements and the related theoretical studies.^{17–20} Nonetheless, the study of those interactions also faces enormous challenges, and understanding the origin of the CDW order in TMDs is still a long-term issue.

Amongst those TMDs, $2H$ -NbSe₂, $2H$ -TaS₂, and $2H$ -TaSe₂ draw more attention because of the coexistence of CDW and superconductivity.^{24–26} These three materials almost have the same properties, and thus are always used as examples to study those collective modes in TMDs. However, in contrast to the other two materials, little attention has been paid toward $2H$ -TaS₂. The major reasons are summarized as follows: The superconducting transition temperature (T_c) of $2H$ -TaS₂ is lower than that of $2H$ -NbSe₂, and the CDW lock-in temperature (T_{CDW}) is lower than that of $2H$ -TaSe₂. Even so, the study of the properties of $2H$ -TaS₂ is also important for understanding the physics of TMDs. The T_{CDW} and T_c of $2H$ -TaS₂ are 78 K and 0.8 K, respectively.^{26,27} Previous works found that the occurrence of CDW orders significantly impacts the internal properties of materials.^{26,28–31} The formation of the CDW order can give rise to some anomalies in heat capacity, specific heat, resistivity, magnetic susceptibility, and so on. Raman spectroscopy is also an efficient and convenient tool to detect

these collective excitations. The redshift of a broad peak, named a soft mode, was found from early Raman measurements.³² Below T_{CDW} , an E_{2g} -symmetric CDW mode was also reported to appear. However, the detailed temperature dependencies of these modes are not analyzed. The origin of the CDW order remains unclear. $2H\text{-TaS}_2$ offers a good opportunity to address the above-mentioned issues.

In this work, we combine the electrical transport and Raman scattering measurements to study the CDW orders in $2H\text{-TaS}_2$. The electrical resistivity, the magneto-resistivity (MR), and the Hall coefficient (R_H) all have anomalies when the sample enters the CDW state. In the Raman scattering measurement, a competitive behavior is observed between the two-phonon mode and the CDW modes. This study is targeted to provide a combined method of electrical transport measurement and Raman spectroscopy to study the CDW order in those materials with strong electron-phonon coupling.

In this experiment, all the data were obtained on fresh surfaces in order to reduce the problem of surface smudginess. The resistivity, magneto-resistivity, and Hall effect measurements were performed using a standard four-point technique on a commercial physical property measurement system (PPMS). Contacts were made with silver paint. All data were taken with a magnetic field perpendicular to the layers.

Raman scattering spectra were obtained in a back-scattering configuration on surfaces with 488 nm and 532 nm sapphire laser beams. The laser beams were focused on the sample by a $\times 20$ objective. In order to reduce the laser heating effect on the sample, the laser powers were stabilized at 0.3 mW for a 488 nm laser and 0.4 mW for a 532 nm laser before the samples. The low-temperature condition was obtained using a specially designed cryostat, and the temperature was measured by a diode mounted near the sample.

The resistivity and MR measurements as a function of temperature were performed from 0.4 K to room temperature (300 K). The results are described in Fig. 1(a). The resistivity rapidly decreases with decreasing temperature. Below T_{CDW} , the resistivity starts to increase, and then decreases more faster upon cooling. Upon further lowering the temperature, the resistivity displays a drop to zero at 0.8 K, as shown in the inset of Fig. 1(a). This signals a superconducting transition. The resistivity under the magnetic field of 9 T was also measured and the MR was calculated using $[R(9\text{ T}) - R(0\text{ T})]/R(0\text{ T})$. The results are shown in a solid blue line in the right of Fig. 1(a). As seen in this figure, the MR is almost constant in the normal state, whereas it drastically increases below T_{CDW} . The details of the low-temperature behavior of the Hall coefficient R_H are shown in Fig. 1(b). As can be seen, R_H above 78 K is positive and almost independent of temperature. Below T_{CDW} , R_H starts to decrease rapidly and changes its sign at a certain temperature. Our findings are similar to those reported data.³¹ The drop in R_H and its sign reversal should also be closely related to the CDW transition. Furthermore, a minimum appears at about 20 K.

Those anomalies in the resistivity, MR, and R_H at around T_{CDW} indicate that the modulation of the electronic structure that resulted from the CDW formation heavily impacts the electronic transport properties. For the sister system $2H\text{-NbSe}_2$, the appearance of the spots at $\frac{2}{3}\Gamma M$ below T_{CDW} was found to be essential to drive the system into an ordered state.^{17,20,33} These spots were suggested to be strongly coupled by CDW modulation. Thus, the electron scattering around these areas is effectively reduced. $2H\text{-TaS}_2$ shares almost the same Fermi surfaces with $2H\text{-NbSe}_2$. This material is also expected to

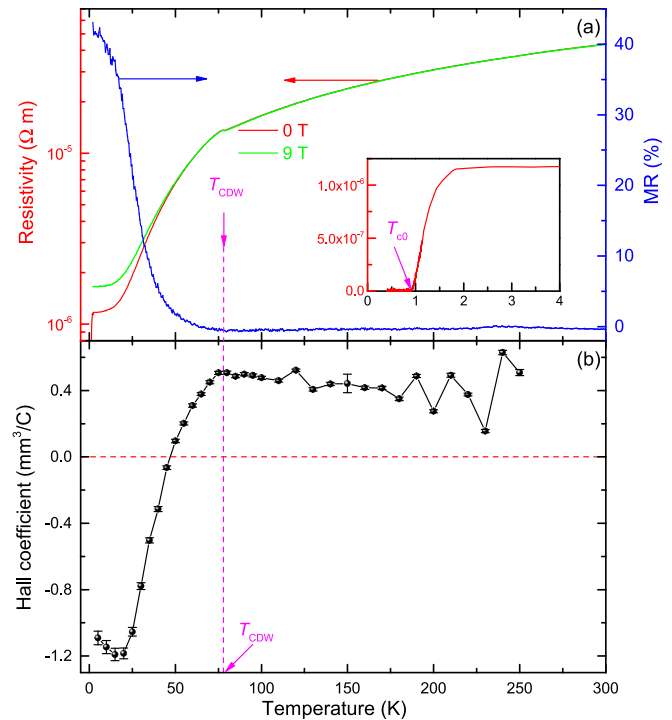


FIG. 1. (a) Temperature dependences of the resistivity (left) and the MR (right) of $2H\text{-TaS}_2$. Anomalies at T_{CDW} are visible and noted by an arrow and a dashed line. Inset presents a zoomed view of the resistivity curve below 4 K. T_{c0} marks the offset T_c . (b) Temperature dependence of the Hall coefficient of $2H\text{-TaS}_2$ from 5 K to 250 K. T_{CDW} is marked by a vertical dashed line.

have a similar modulation below T_{CDW} .^{20,33} These ordered areas available enhance the electrical transport properties. As a result, this material becomes more metallic in the CDW state even though a portion of the FS is gapped. The hump structure in the R-T curve around T_{CDW} might result from the modification of the FS. This scenario agrees with the previous electrical transport measurement of the $2H$ TMDs. The resistivity behavior is explained by using the two-band model. Otherwise, the modulation on the FS should also result in the anomalies of the MR. The anomalies of the Hall coefficient can be well explained by the geometric interpretation developed by Ong.^{34–36} The strongly coupled portion is located at the areas of electron pockets.^{17,33} Thus, the mean free path of electrons increases drastically. However, the holes behave differently. Their mean free path has only a modest increase.³⁶ Consequently, the R_H decreases after the CDW modulation.

The crystal structure of $2H\text{-TaS}_2$ is hexagonal D_{6h}^4 . Thus, the Raman active modes are A_{1g} , E_{1g} , and E_{2g} .^{37,38} The details of the schematic diagram of each mode are shown in Fig. 2(a).

The E_{2g}^2 mode is a common mode in the layered materials. This mode comes from the relative motions between neighboring layers. This rigid-layer mode has an energy of about 27 cm^{-1} at room temperature. The energies of another two modes, E_{2g}^1 and A_{1g} are at 286 cm^{-1} and 400 cm^{-1} , respectively. Another Raman active mode E_{1g} cannot be observed; it is presumably because of the small Raman cross-section.³² In addition, a broad two-phonon scattering mode is

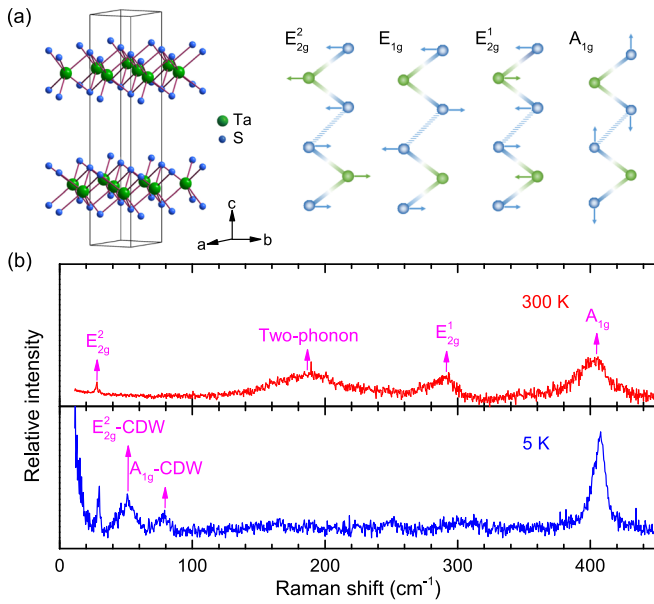


FIG. 2. Raman active vibrational modes of 2H-TaS₂. (a) Schematic diagrams of the A_{1g}, E_{1g}, and E_{2g} modes for one-phonon processes. The 2H polytype contains two layers per unit cell. (b) Raman spectra at 300 K and 5 K excited by a 532 nm laser. Each peak has been marked by a short arrow.

observed at about 195 cm⁻¹. This mode is common to the 2H-compounds with CDW phase transitions. At temperatures below T_{CDW}, several new peaks appear at around 48 cm⁻¹ (E_{2g}¹-mode) and 75 cm⁻¹ (A_{1g}¹-mode). These modes are suggested to correspond to the Raman active amplitude excitations of the CDW orders.^{32,39}

Raman spectra at different temperatures are measured by the 532 and 488 nm laser excitations. In order to analyze the vibration modes, we removed a constant background from the raw data. Then, we normalized the scattering intensity by the statistical factor *n* for the Stokes side by $I(\omega) = I_0(\omega) / [n(\omega, T) + 1]$, where $n(\omega, T)$ is the Bose-Einstein distribution function evaluated at mode energy ω and temperature *T*, and $I_0(\omega)$ is the observed intensity. The normalized

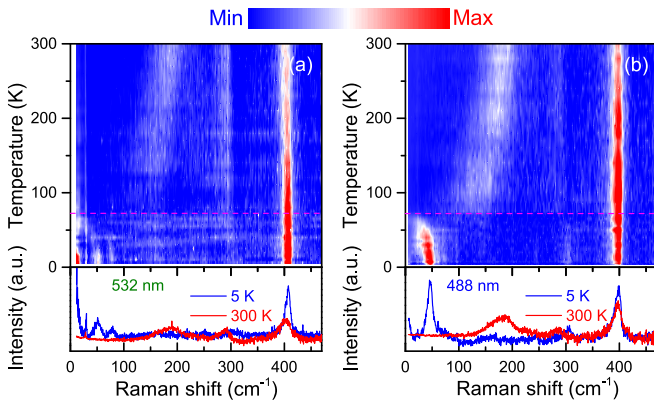


FIG. 3. Temperature maps of the Raman scattering intensity excited by (a) the 532 nm and (b) 488 nm lasers. The spectra at 5 K and 300 K are presented for clarification.

Raman spectral maps are shown in Fig. 3. The frequency distinctions of the vibrational modes between these two spectra should result from different calibration accuracies.

These two maps almost show the same behavior. The three modes E_{2g}¹, E_{2g}², and A_{1g} exhibit blueshifts with decreasing temperature, and their intensities also simultaneously increase. Meanwhile, both the frequency and the intensity of the two-phonon mode decrease with decreasing temperature. Below T_{CDW}, the two-phonon mode disappears. Upon cooling, the CDW amplitude modes appear. Interestingly, these two spectra show a different scenario. Below T_{CDW}, two CDW modes appear in the 532 nm laser excited spectra. In contrast, the A_{1g}-CDW mode almost disappears in the 488 nm laser excited spectra, and only a weak tail can be observed on the right of the E_{2g}-CDW. The A_{1g}-CDW was mentioned in the early Raman scattering measurement that this mode can hardly be observed due to the weak intensity and the broad spectral width.³² However, our work discovers that the E_{2g}-DW mode is very sensitive to the applied excitation energy. The intensity of this mode excited by a higher energy laser is stronger than the low energy laser excited intensity. The intensity is even higher than the A_{1g} mode [see the Raman spectrum at 5 K in Fig. 3(b)]. The A_{1g}-CDW is less sensitive to the laser energy. Thus, the weak A_{1g}-CDW excited by the 488 nm laser drowns in the E_{2g}-CDW. The energies of these two CDW modes all increase with decreasing temperature.

Lorentzian function is used to analyze the detailed vibration properties of those modes, and the results are presented in Figs. 4 and 5. The E_{2g}² modes can hardly be fitted due to the weak intensity. The E_{2g}¹ modes excited by the 532 nm and 488 nm lasers show almost the same behaviors above T_{CDW}. Below T_{CDW}, the energy of the former mode monotonously increases, whereas the latter shows a drastic increase and then becomes constant. The A_{1g} modes in these two Raman spectra show unusual behaviors. The A_{1g} mode in the spectra excited by the 532 nm laser shows an obvious blueshift from 401 cm⁻¹ at room temperature to 407 cm⁻¹ at 7 K. However, in the 488 nm laser excited Raman spectra without the appearance of A_{1g}-CDW, the energy of the A_{1g} mode is almost a constant, and this mode moves less

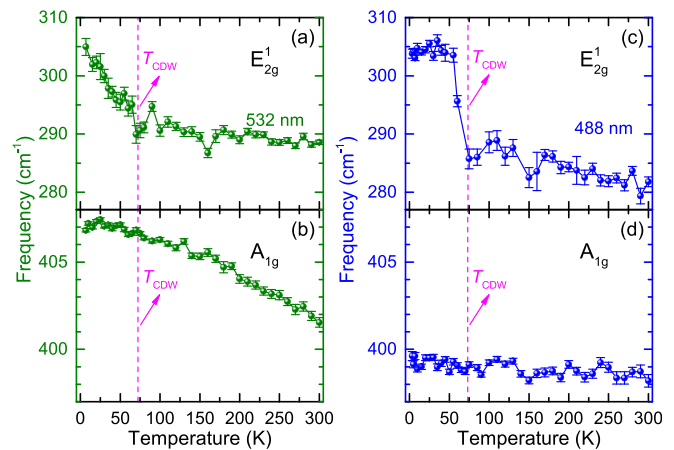


FIG. 4. Temperature dependences of the frequencies of the E_{2g}¹ and A_{1g} modes. (a) and (b) are the results with the excitation of the 532 nm laser. (c) and (d) are the results with the excitation of the 488 nm laser. The CDW transition temperature is pointed out by pink lines and arrows.

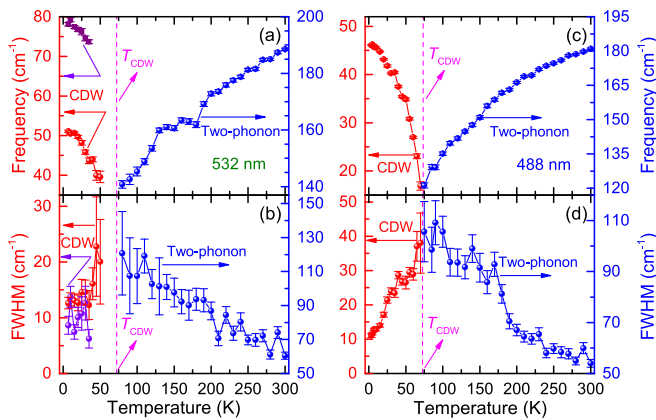


FIG. 5. Temperature dependences of the frequencies and the FWHM values of the E_{2g} -CDW, A_{1g} -CDW, and two-phonon modes. (a) and (b) are the results with the excitation of the 532 nm laser. (c) and (d) are the results with the excitation of the 488 nm laser. The CDW transition temperature is pointed out by pink lines and arrows.

than 1 cm^{-1} . The distinctions indicate that the A_{1g} mode is also sensitive to the applied excitation energy, and this mode is seemingly connected to the A_{1g} -CDW mode. In addition, as shown in this figure, one can see that the A_{1g} peaks in the former spectra are always excellent Lorentzian profile peaks in the full temperature range, whereas in the latter spectra, this peak becomes increasingly asymmetric. This situation should result from the Fano resonance.⁴⁰

The frequencies and FWHM values of the two-phonon modes and CDW modes as a function of temperature are presented in Fig. 5. The two-phonon mode always draws a lot of attention due to the extraordinary correlation with CDW orders. The energies of the two-phonon modes decrease with decreasing temperature. Meanwhile, their FWHM values increase and the intensities decrease. Interestingly, the soft modes absolutely disappear at T_{CDW} . Below T_{CDW} , the E_{2g} -symmetric and A_{1g} -symmetric CDW modes appear, and their energies increase with decreasing temperature. The growth rate gradually decreases, and the extrapolated energies to 0 K are 50 cm^{-1} for the E_{2g} -CDW and 80 cm^{-1} for the A_{1g} -CDW, respectively. These anomalies at around T_{CDW} indicate that there are some competitive relations between the two-phonon mode and CDW modes.

Recent inelastic X-ray scattering experiments¹⁸ measured the temperature dependence of phonon dispersion in the prototypical charge-density-wave compound $2H\text{-NbSe}_2$. They discovered that a broad dispersion anomaly appears at q_{CDW} . This anomaly deepens considerably upon cooling to T_{CDW} , and the damping strongly increases. However, below T_{CDW} , the energies become hardened and the damping reduced. The frequency of the two-phonon mode is revealed to be approximately twice that of a broad dip or anomaly in the dispersion curves of the longitudinal-acoustic (LA) phonon near a wave vector $q = \frac{2}{3}\Gamma M$.⁴¹ Consequently, the damping here directly impacts the energy of the two-phonon mode, to wit, the two-phonon mode is also damped from the normal state on approaching the CDW phase taking the interaction with d -electrons near the Fermi energy of Ta into account.⁴¹ Below T_{CDW} , the CDW mode appears, hardens, and narrows with decreasing temperature, as seen in Fig. 5. This

results from the growing electron-phonon coupling in this material.^{17,18,20} Meanwhile, the damping also impacts the anharmonicity of the two-phonon mode, so the FWHM of the two-phonon mode increases.

In summary, we have reported a combined study of electrical transport measurements and Raman scattering spectroscopy of $2H\text{-TaS}_2$ at low temperatures. The resistivity, the magneto-resistivity, and the Hall coefficient all show significant changes at around the CDW lock-in temperature. Such a phenomenon is suggested to result from the modulation of the electron pockets in the CDW state. Below T_{CDW} , the mean-free path of electrons increases drastically. This increase results in the occurrence of an anomaly in the magneto-resistivity, as well as a sharp drop in the Hall coefficient. Meanwhile, our Raman data show a softening behavior of the two-phonon peak at low temperatures. This phenomenon should result from the increasing damping caused by the strong electron-phonon interactions on the soft-mode branch with decreasing temperature. As the CDW formation occurs below T_{CDW} , the two-phonon peak disappears and the CDW peaks appear. In addition, the E_{2g} -CDW mode is found to be more sensitive to the energy of the excitation. The properties of the CDW in other types of materials with superconductivity such as high- T_c cuprate superconductors with strong electron-phonon coupling are also highly attractive. Our study provides a combined method of electrical transport and Raman spectroscopy measurements to study the CDW order in those materials.

REFERENCES

- E. Gibney, "The super materials that could trump graphene," *Nat. News* **522**, 274 (2015).
- A. Wilson, F. J. Di Salvo, and S. Mahajan, "Charge-density waves and superlattices in the metallic layered transition metal dichalcogenides," *Adv. Phys.* **24**, 117–201 (1975).
- R. Grasset, T. Cea, Y. Gallais, M. Cazayous, A. Sacuto, L. Cario, L. Benfatto, and M. A. Méasson, "Higgs-mode radiance and charge-density-wave order in $2H\text{-NbSe}_2$," *Phys. Rev. B* **97**, 094502 (2018).
- R. Sooryakumar and M. V. Klein, "Raman scattering by superconducting-gap excitations and their coupling to charge-density waves," *Phys. Rev. Lett.* **45**, 660–662 (1980).
- M. A. Méasson, Y. Gallais, M. Cazayous, B. Clair, P. Rodiere, L. Cario, and A. Sacuto, "Amplitude Higgs mode in the $2H\text{-NbSe}_2$ superconductor," *Phys. Rev. B* **89**, 060503 (2014).
- X. Li, C. Q. Wu, and D. H. Lee, "Checkerboard charge density wave and pseudogap of high- T_c cuprate," *Phys. Rev. B* **74**, 184515 (2006).
- W. D. Wise, M. C. Boyer, K. Chatterjee, T. Kondo, T. Takeuchi, H. Ikuta, Y. Wang, and E. W. Hudson, "Charge-density-wave origin of cuprate checkerboard visualized by scanning tunnelling microscopy," *Nat. Phys.* **4**, 696–699 (2008).
- T. Wu, H. Mayaffre, S. Krämer, M. Horvatić, C. Berthier, W. N. Hardy, R. Liang, D. A. Bonn, and M. H. Julien, "Magnetic-field-induced charge-stripe order in the high-temperature superconductor $\text{YBa}_2\text{Cu}_3\text{O}_y$," *Nature* **477**, 191–194 (2011).
- A. A. Kordyuk, S. V. Borisenko, V. B. Zabolotnyy, R. Schuster, D. S. Inosov, D. V. Evtushinsky, A. I. Plyushchay, R. Follath, A. Varykhalov, L. Patthey, and H. Berger, "Nonmonotonic pseudogap in high- T_c cuprates," *Phys. Rev. B* **79**, 020504 (2009).
- S. V. Borisenko, A. A. Kordyuk, A. N. Yaresko, V. B. Zabolotnyy, D. S. Inosov, R. Schuster, B. Büchner, R. Weber, R. Follath, L. Patthey, and H. Berger, "Pseudogap and charge density waves in two dimensions," *Phys. Rev. Lett.* **100**, 196402 (2008).
- T. M. Rice and G. K. Scott, "New mechanism for a charge-density-wave instability," *Phys. Rev. Lett.* **35**, 120–123 (1975).

- ¹²T. Kiss, T. Yokoya, A. Chainani, S. Shin, T. Hanaguri, M. Nohara, and H. Takagi, "Charge-order-maximized momentum-dependent superconductivity," *Nat. Phys.* **3**, 720–725 (2007).
- ¹³S. V. Borisenko, A. A. Kordyuk, V. B. Zabolotnyy, D. S. Inosov, D. Evtushinsky, B. Büchner, A. N. Yaresko, A. Varykhalov, R. Follath, W. Eberhardt, L. Patthey, and H. Berger, "Two energy gaps and Fermi-surface "arcs" in NbSe₂," *Phys. Rev. Lett.* **102**, 166402 (2009).
- ¹⁴Th. Straub, Th. Finteis, R. Claessen, P. Steiner, S. Hüfner, P. Blaha, C. S. Oglesby, and E. Bucher, "Charge-density-wave mechanism in 2H-NbSe₂: Photoemission results," *Phys. Rev. Lett.* **82**, 4504–4507 (1999).
- ¹⁵M. N. Faraggi, X. Zubizarreta, A. Arnau, and V. M. Silkin, "On the stability of the electronic system in transition metal dichalcogenides," *J. Phys.: Condens. Matter* **28**, 184004 (2016).
- ¹⁶C. J. Arguello, S. P. Chockalingam, E. P. Rosenthal, L. Zhao, C. Gutiérrez, J. H. Kang, W. C. Chung, R. M. Fernandes, S. Jia, A. J. Millis, R. J. Cava, and A. N. Pasupathy, "Visualizing the charge density wave transition in 2H-NbSe₂ in real space," *Phys. Rev. B* **89**, 235115 (2014).
- ¹⁷T. Valla, A. V. Fedorov, P. D. Johnson, P. A. Glans, C. McGuinness, K. E. Smith, E. Y. Andrei, and H. Berger, "Quasiparticle spectra, charge-density waves, superconductivity, and electron-phonon coupling in 2H-NbSe₂," *Phys. Rev. Lett.* **92**, 086401 (2004).
- ¹⁸F. Weber, S. Rosenkranz, J. P. Castellan, R. Osborn, R. Hott, R. Heid, K. P. Bohnen, T. Egami, A. H. Said, and D. Reznik, "Extended phonon collapse and the origin of the charge-density wave in NbSe₂," *Phys. Rev. Lett.* **107**, 107403 (2011).
- ¹⁹X. Zhu, Y. Cao, J. Zhang, E. W. Plummer, and J. Guo, "Classification of charge density waves based on their nature," *Proc. Natl. Acad. Sci. U. S. A.* **112**, 2367–2371 (2015).
- ²⁰K. Wijayarathne, J. Zhao, C. Malliakas, D. Y. Chung, M. G. Kanatzidis, and U. Chatterjee, "Spectroscopic signature of moment-dependent electron-phonon coupling in 2H-TaS₂," *J. Mater. Chem. C* **5**, 11310–11316 (2017).
- ²¹D. J. Rahn, S. Hellmann, M. Källäne, C. Sohr, T. K. Kim, L. Kipp, and K. Rossnagel, "Gaps and kinks in the electronic structure of the superconductor 2H-NbSe₂ from angle-resolved photoemission at 1 K," *Phys. Rev. B* **85**, 224532 (2012).
- ²²M. D. Johannes, I. I. Mazin, and C. A. Howells, "Fermi-surface nesting and the origin of the charge-density wave in NbSe₂," *Phys. Rev. B* **73**, 205102 (2006).
- ²³K. Rossnagel, O. Seifarth, L. Kipp, M. Skibowski, D. Voß, P. Krüger, A. Mazur, and J. Pollmann, "Fermi surface of 2H-NbSe₂ and its implications on the charge-density-wave mechanism," *Phys. Rev. B* **64**, 235119 (2001).
- ²⁴P. M. Williams, C. B. Scruby, and G. J. Tatlock, "Charge density waves in 2H-NbSe₂," *Solid State Commun.* **17**, 1197–1200 (1975).
- ²⁵D. E. Moncton, J. D. Axe, and F. J. DiSalvo, "Neutron scattering study of the charge-density wave transitions in 2H-TaS₂ and 2H-NbSe₂," *Phys. Rev. B* **16**, 801–819 (1977).
- ²⁶J. P. Tidman, O. Singh, A. E. Curzon, and R. F. Frindt, "The phase transition in 2H-TaS₂ at 75 K," *Philos. Mag.* **30**, 1191–1194 (1974).
- ²⁷S. Nagata, T. Aochi, T. Abe, S. Ebisu, T. Hagino, Y. Seki, and K. Tsutsumi, "Superconductivity in the layered compound 2H-TaS₂," *J. Phys. Chem. Solids* **53**, 1259–1263 (1992).
- ²⁸S. J. Hillenius and R. V. Coleman, "Quantum oscillations and the Fermi surface of 2H-TaS₂," *Phys. Rev. B* **18**, 3790–3798 (1978).
- ²⁹J. M. E. Harper, T. H. Geballe, and F. J. DiSalvo, "Thermal properties of layered transition-metal dichalcogenides at charge-density-wave transitions," *Phys. Rev. B* **15**, 2943–2951 (1977).
- ³⁰P. Goroche, P. Manuel, J. J. Veysié, and P. Molinié, "Dynamic measurements of the low-temperature specific heat of 2H-TaS₂ single crystals in magnetic fields," *J. Low Temp. Phys.* **30**, 323–336 (1978).
- ³¹M. Naito and S. Tanaka, "Electrical transport properties in 2H-NbS₂, -NbSe₂, -TaS₂ and -TaSe₂," *J. Phys. Soc. Jpn.* **51**, 219–227 (1982).
- ³²S. Sugai, K. Murase, S. Uchida, and S. Tanaka, "Studies of lattice dynamics in 2H-TaS₂ by Raman scattering," *Solid State Commun.* **40**, 399–401 (1981).
- ³³J. Zhao, K. Wijayarathne, A. Butler, J. Yang, C. D. Malliakas, D. Y. Chung, D. Louca, M. G. Kanatzidis, J. van Wezel, and U. Chatterjee, "Orbital selectivity causing anisotropy and particle-hole asymmetry in the charge density wave gap of 2H-TaS₂," *Phys. Rev. B* **96**, 125103 (2017).
- ³⁴N. P. Ong, "Geometric interpretation of the weak-field Hall conductivity in two-dimensional metals with arbitrary Fermi surface," *Phys. Rev. B* **43**, 193–201 (1991).
- ³⁵A. P. Mackenzie, N. E. Hussey, A. J. Diver, S. R. Julian, Y. Maeno, S. Nishizaki, and T. Fujita, "Hall effect in the two-dimensional metal Sr₂RuO₄," *Phys. Rev. B* **54**, 7425 (1996).
- ³⁶L. Li, J. Shen, Z. Xu, and H. Wang, "Magnetoresistance and Hall effect of two-dimensional 2H-NbSe₂," *Int. J. Mod. Phys. B* **19**, 275–279 (2005).
- ³⁷A. Meetsma, G. A. Wiegers, R. J. Haange, and J. L. De Boer, "Structure of 2H-TaS₂," *Acta Cryst. C* **46**, 1598–1599 (1990).
- ³⁸W. G. McMullan and J. C. Irwin, "Long-wavelength phonons in 2H-NbS₂, 2H-TaS₂, and Ag_xTaS₂," *Can. J. Phys.* **62**, 789–795 (1984).
- ³⁹J. C. Tsang, J. E. Smith, and M. W. Shafer, "Raman spectroscopy of soft modes at the charge-density-wave phase transition in 2H-NbSe₂," *Phys. Rev. Lett.* **37**, 1407–1410 (1976).
- ⁴⁰J. Bäckström, M. Rübhausen, M. Käll, L. Börjesson, A. P. Litvinchuk, M. Kakihana, M. Osada, and B. Dabrowski, "Raman scattering in YBa₂Cu₄O₈ and PrBa₂Cu₄O₈: Indications of pseudogap effects in nonsuperconducting PrBa₂Cu₄O₈," *Phys. Rev. B* **61**, 7049–7054 (2000).
- ⁴¹M. V. Klein, "Theory of two-phonon Raman scattering in transition metals and compounds," *Phys. Rev. B* **24**, 4208–4223 (1981).